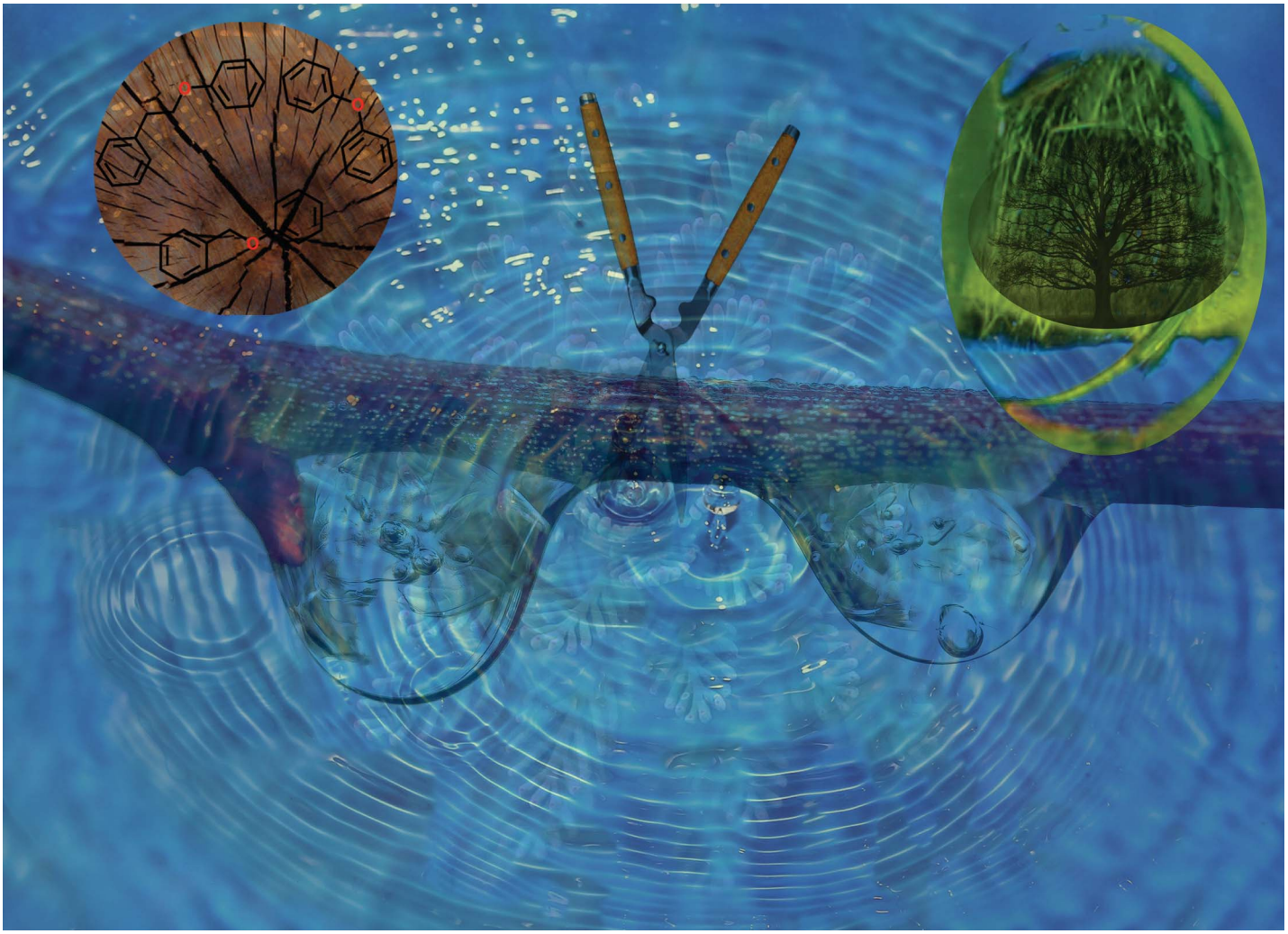

Showcasing research from Professor Paul J. Dyson's laboratory, Institute of Chemical Sciences and Engineering, Ecole Polytechnique Fédérale de Lausanne, Switzerland and Professor Ning Yan's laboratory, Department of Chemical and Biomolecular Engineering, National University of Singapore.

Efficient cleavage of aryl ether C–O linkages by Rh–Ni and Ru–Ni nanoscale catalysts operating in water

Water dispersed bimetallic Ru–Ni and Rh–Ni nanocatalysts efficiently cleave aryl ether C–O linkages in the presence of hydrogen. The impact of the metal combination on the efficiency of the hydrogenolysis reaction and the competing hydrogenation reaction is evaluated, and mechanistic insights into the reaction pathways are provided. The bimetallic nanocatalysts are also shown to catalyse the delignification of beech wood.

As featured in:

See Paul J. Dyson *et al.*, *Chem. Sci.*, 2018, **9**, 5530.

ROYAL SOCIETY OF CHEMISTRY

rsc.li/chemical-science

Registered charity number: 207890

Chemical Science

EDGE ARTICLE

View Article Online
View Journal | View Issue

Cite this: *Chem. Sci.*, 2018, **9**, 5530

Efficient cleavage of aryl ether C–O linkages by Rh–Ni and Ru–Ni nanoscale catalysts operating in water†

Safak Bulut,[a] Sviatlana Siankevich,[a] Antoine P. van Muyden,[a] Duncan T. L. Alexander,[b] Georgios Savoglidis,[a] Jiaguang Zhang,[c] Vassily Hatzimanikatis,[a] Ning Yan[c] and Paul J. Dyson*[a]

Received 13th February 2018
Accepted 29th May 2018

DOI: 10.1039/c8sc00742j

rsc.li/chemical-science

Bimetallic Ru–Ni and Rh–Ni nanocatalysts coated with a phase transfer agent efficiently cleave aryl ether C–O linkages in water in the presence of hydrogen. For dimeric substrates with weaker C–O linkages, *i.e.* α-*O*-4 and β-*O*-4 bonds, low loadings of the precious metal (Rh or Ru) in the nanocatalysts quantitatively afford monomers, whereas for the stronger 4-*O*-5 linkage higher amounts of the precious metal are required to achieve complete conversion. Under the optimized, relatively mild operating conditions, the C–O bonds in a range of substituted ether compounds are efficiently cleaved, and mechanistic insights into the reaction pathways are provided. This work paves the way to sustainable approaches for the hydrogenolysis of C–O bonds.

The hydrogenolysis of aryl ether and other types of C–O bonds is highly challenging because of their relatively high bond dissociation energies and the competition with alternative hydrogenation reactions.[1] However, due to increased interest in the valorization of the lignin component of biomass, an abundant renewable polymer comprising aromatic units held together by various types of C–O bonds, the need for efficient and selective hydrogenolysis catalysts is essential for biomass valorisation.[2] Indeed, the enormous amount of waste lignin available offers a renewable raw material that could potentially rival coal tar and petroleum as a viable source of aromatic and cyclic hydrocarbons,[3] and would therefore contribute towards reducing CO_2 emissions and the associated environmental problems.[4] Lignin is an integral part of cell walls of ligneous plants and has a protective function against hydrolytic and biological degradation.[5] Consequently, lignin is a very stable, robust polymer that is difficult to breakdown.[6] In lignin three different types of C–O linkages are dominant, *i.e.* α-*O*-4, β-*O*-4 and 4-*O*-5 linkages (Fig. 1).[7]

A wide range of heterogeneous noble metal[10] and non-noble metal catalysts[11] have been reported for the hydrogenolysis of the substrates illustrated in Fig. 1. These catalysts tend to operate only at elevated temperatures (typically above 120 °C for noble metal catalysts and above 200 °C for non-noble metal catalysts) and under elevated pressures of H_2 (≥10 atm). Several recent reports describe catalysts that operate under somewhat less forcing conditions,[11c,12] including Ni-based homogenous and heterogenous catalysts reported by Hartwig and coworkers.[13] Initially, they used a homogenous system generated *in situ* from $Ni(COD)_2$ and a N-heterocyclic carbene in the presence of an excess of NaO^tBu.[13a] However, high catalyst loadings (20 mol% of $Ni(COD)_2$ and 40 mol% of N-heterocyclic carbene) were required and, they subsequently showed that lower catalyst loadings could be achieved using Ni nanoparticles that formed *in situ* from $Ni(COD)_2$ in the presence of an excess of NaO^tBu.[13b,13c] These reactions operate under inert conditions in dry organic solvents at temperatures between 120–140 °C. Recent work from the same group demonstrates the

[a]*Institut des Sciences et Ingénierie Chimiques, Ecole Polytechnique Fédérale de Lausanne (EPFL), 1015, Lausanne, Switzerland. E-mail: paul.dyson@epfl.ch*
[b]*Interdisciplinary Centre for Electron Microscopy (CIME), Ecole Polytechnique Fédérale de Lausanne (EPFL), 1015, Lausanne, Switzerland*
[c]*Department of Chemical and Biomolecular Engineering, National University of Singapore, 4 Engineering Drive 4, 117576, Singapore*

† Electronic supplementary information (ESI) available: Experimental details, powder XRD and XPS analysis, details for catalytic studies and results, ICP results, TEM analysis of the catalysts (before and after reaction), catalytic results with shorter reaction times and details for thermodynamic calculations. See DOI: 10.1039/c8sc00742j

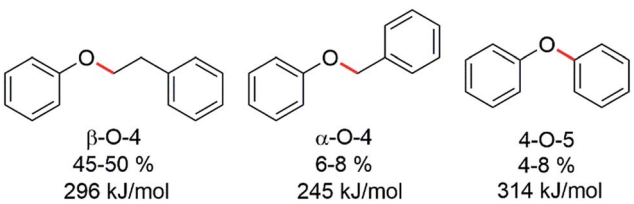

Fig. 1 The three main C–O linkages present in lignin together with their approximate abundance[8] and C–O bond dissociation energies[9a] illustrated using key model compounds.

importance of using an excess of strong base,[14] even when using the pre-synthesized Ni(SIPr)$_2$ (SIPr = 1,3-bis-(2,6-diisopropylphenyl)imidazolinium chloride) catalyst that was generated *in situ* in the initial report.[13a] It should be noted that the separation of water from raw biomass is difficult and costly and, consequently, air and moisture stable catalytic methodologies would be advantageous for the valorization of real biomass.

Here, we describe a series of Ru–Ni and Rh–Ni nanocatalysts (NCs) coated with a phase transfer agent that catalyse the hydrogenolysis of even the least reactive 4-*O*-5 linkage in diphenyl ether at lower temperatures, below 100 °C and under 1 atm of H_2, with a relative low catalyst loading of 5 mol%, using water as the reaction medium (both for the synthesis of NCs and catalytic reactions), without using any additives, *e.g.* a base ruthenium–nickel $Ru_{100-x}Ni_x$ and rhodium–nickel $Rh_{100-x}Ni_x$ NCs, where x is the molar percentage of Ni used in the synthesis, were prepared in water from the reduction of $RuCl_3$, $RhCl_3$ or $NiCl_2$, or their combinations, with $NaBH_4$ in the presence of cetyltrimethylammonium bromide (CTAB), employed as both a stabilizing agent and a phase transfer reagent. The $Ru_{15}Ni_{85}$ and $Rh_{15}Ni_{85}$ NCs (selected as they exhibit the optimum catalytic activity, see below) were characterized using transmission electron microscopy (TEM), high angle annular dark field (HAADF) scanning transmission electron microscopy combined with energy-dispersive X-ray spectroscopy (STEM-EDS) mapping (Fig. 2), and powder X-ray diffraction (XRD), X-ray photoelectron spectroscopy (XPS) (Fig. S1–S3†). The material is unstable under the extended electron beam exposure of STEM-EDS mapping, for instance with a tendency of neighbouring NCs to coalesce together (Fig. S4†).

Consequently, the acceleration voltage and probe current were reduced to minimise this effect (80 kV and ~0.5 nA respectively), and only data representative of the initial sample state are shown. Images and EDS maps for the $Ru_{15}Ni_{85}$ and $Rh_{15}Ni_{85}$ samples (Fig. 2) reveal a morphology comprising of NCs that are consistent with a bimetallic nature of Ru–Ni or Rh–Ni (depending on the sample), dispersed on thin, more homogeneous membrane-like structures, which contain mostly Ni (Fig. S5†). These membranes aggregate into larger, porous structures, and EDS shows that they also contain O, Cl and Br (Fig. S6†). The $Ru_{15}Ni_{85}$ NCs have an average size of 2.0 ± 0.2 nm whereas the $Rh_{15}Ni_{85}$ NCs are slightly larger, average diameter = 2.7 ± 0.3 nm (Fig. 2). Their compositions were also confirmed by inductively coupled plasma mass spectrometry (ICP-MS, see ESI†).

The catalytic activity of the NCs was evaluated in the hydrogenolysis of three lignin model substrates using water as a solvent (Fig. 1). At a catalyst loading of 5 mol% (based on metal content) quantitative cleavage of the C–O linkages was obtained at 95 °C under 1 atm of H_2 in 16 hours, depending on the metal–nickel (metal = Ru or Rh) molar ratio (see Fig. 3, 4 and Tables S2–S7†). Compounds with only one C_6-ring derived from the hydrogenolysis of the C–O bond are denoted as monomers whereas dimer products are generated by hydrogenation of the substrate without the cleavage of the C–O bond. As expected, conversion of the β-*O*-4 and α-*O*-4 linkage containing substrates (Fig. 3 and 4, respectively) to monomers is easier to achieve than hydrogenolysis of diphenyl ether, which contains the 4-*O*-5 linkage.

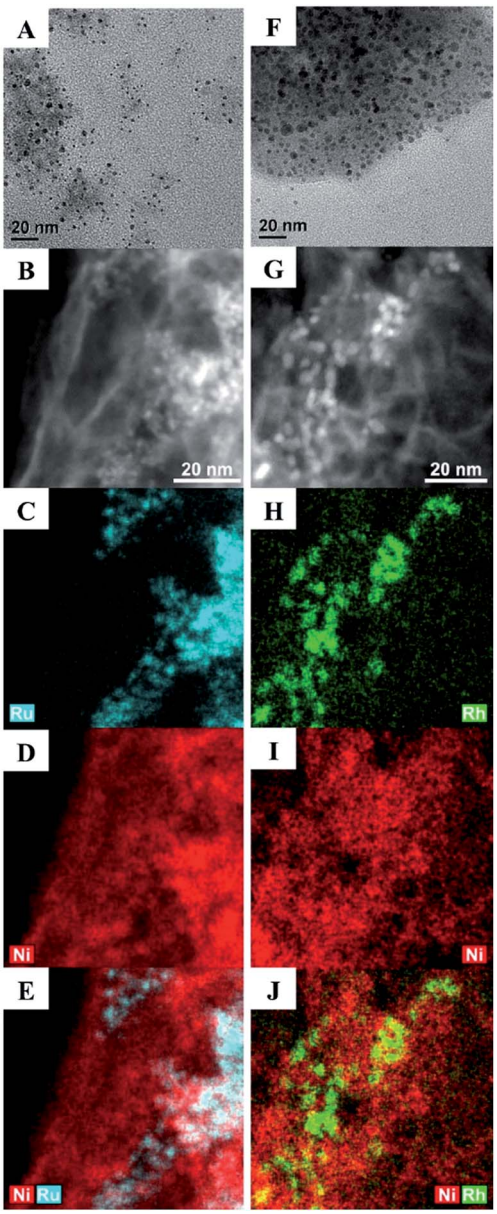

Fig. 2 TEM (A and F), and HAADF STEM (B and G) and corresponding EDS maps (C–E and H–J) for the (left) $Ru_{15}Ni_{85}$ and (right) $Rh_{15}Ni_{85}$ materials. The NCs appear brighter on the Z-contrast HAADF images. Note that the scale of the EDS maps is the same as that in the HAADF STEM images.

The bimetallic NCs containing only low amounts of Ru and Rh result in complete conversion of the α-*O*-4 and β-*O*-4 linkage containing substrates. In contrast, a relative high molar ratio of the precious metal was required to achieve near-quantitative cleavage of the 4-*O*-5 bond. Notably, the bimetallic NCs afford higher monomer yields under milder conditions than other reported bimetallic NCs containing Ni.[10c]

Ethylbenzene is the major product resulting from the cleavage of the β-*O*-4 bond for all the bimetallic catalyst, in the

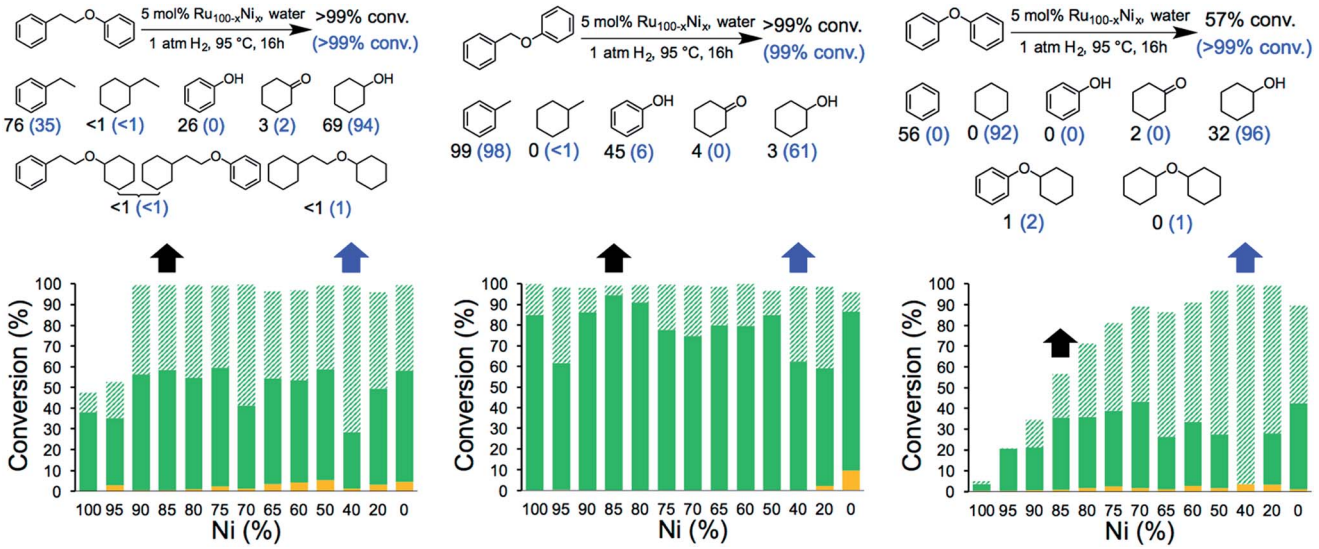

Fig. 3 Hydrogenolysis/hydrogenation of (left) 1-phenoxy-2-phenylethane (β-*O*-4 linkage), (middle) benzyl phenyl ether (α-*O*-4 linkage), (right) diphenyl ether (4-*O*-5 linkage) and product yield for selected metal combinations catalysed by $Ru_{100-x}Ni_x$ NCs. Full details are provided in Tables S2, S4 and S6.† The black arrows refer to the $M_{15}Ni_{85}$ NCs and the corresponding yields are in black. The blue arrows refer to the $M_{60}Ni_{40}$ NCs and the corresponding yields are in blue in parenthesis. The fractions comprise partially/fully hydrogenated dimers (■), non-hydrogenated monomers (■) and hydrogenated monomers (▨).

best case, *i.e.* with the $Rh_{15}Ni_{85}$ NC catalyst, reaching close to the maximum (96%). Significant differences in the relative amounts of phenol and cyclohexanol are observed with the different catalysts. In general, the $Ru_{15}Ni_{85}$ catalyst is able to hydrogenate the phenol ring more efficiently than the $Rh_{15}Ni_{85}$ catalyst (69 *vs.* 27% yield, respectively). Raising the content of noble metal to 60% leads to an increase in the total amount of hydrogenated products, indicating that the noble metal is primarily responsible for hydrogenation of the aromatic rings, as observed elsewhere.[15] A similar trend was noted for the α-*O*-4 substrate. Since the β-*O*-4 and α-*O*-4 linkages are almost completely converted after 16 h reaction time, the NCs were also evaluated at shorter reaction times, *i.e.* 4 hours for the β-*O*-4 linkage and 1 hour for α-*O*-4 linkage (see Fig. S13†). At these shorter reaction times, mostly monomer products were observed, implying that the hydrogenation of the rings tends to

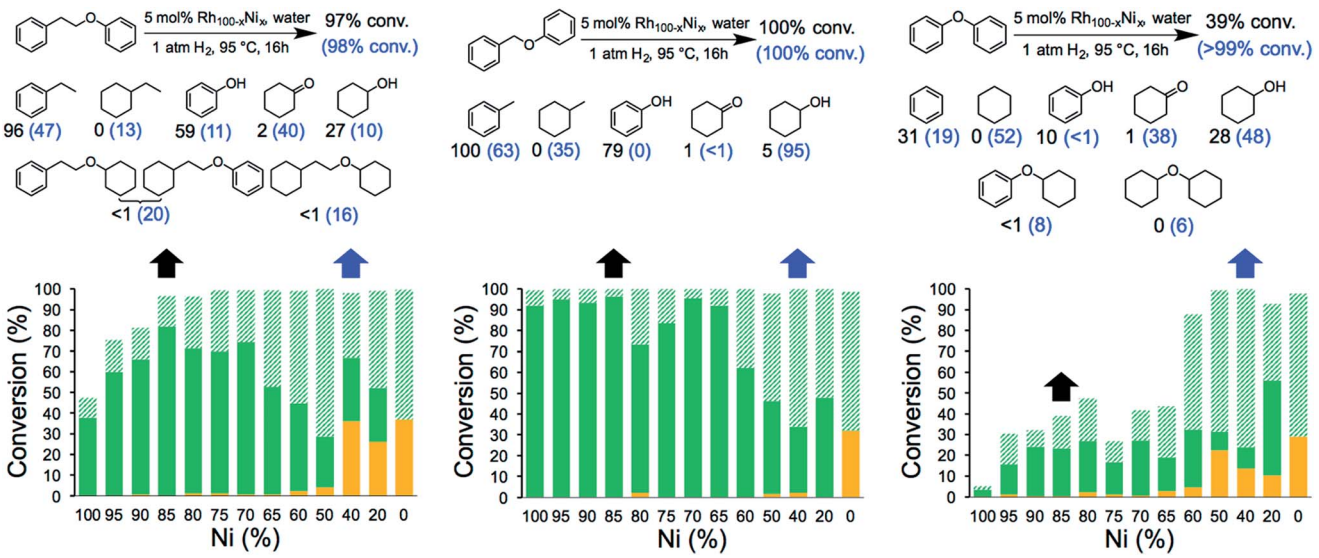

Fig. 4 Hydrogenolysis/hydrogenation of (left) 1-phenoxy-2-phenylethane (β-*O*-4 linkage), (middle) benzyl phenyl ether (α-*O*-4 linkage), (right) diphenyl ether (4-*O*-5 linkage) and product yield for selected metal combinations catalysed by $Rh_{100-x}Ni_x$ NCs. Full details are provided in Tables S3, S5 and S7.† The black arrows refer to the $M_{15}Ni_{85}$ NCs and the corresponding yields are in black. The blue arrows refer to the $M_{60}Ni_{40}$ NCs and the corresponding yields are in blue in parenthesis. The fractions comprise partially/fully hydrogenated dimers (■), non-hydrogenated monomers (■) and hydrogenated monomers (▨).

take place after the hydrogenolysis. With the substrates containing the β-*O*-4 and α-*O*-4 linkages the best activities were observed for the RuNi NCs containing 85–90 and 75–85% Ni, respectively. In contrast with the RhNi NCs higher conversions are obtained at high loadings of Rh, *i.e.* 60–80% Rh.

The hydrogenolysis of diphenyl ether is more challenging than the other two substrates due to the higher bond dissociation energy of the 4-*O*-5 linkage.[16] Nevertheless, at higher ratios of noble metal, *i.e.* $M_{60}Ni_{40}$ (where M = Ru or Rh), both bimetallic systems favor the formation of monomers (>90%), with cyclohexane and cyclohexanol obtained in 92 and 96% yield, respectively, with the $Ru_{60}Ni_{40}$ nanocatalyst. At lower noble metal contents substrate conversion is significantly reduced (Fig. 3 and 4). Moreover, these nanocatalysts result in higher monomer yields compared to commercial Ru/C, Rh/C and RANEY® Ni catalysts (Table S1†).

The morphology and composition of the catalyst was analysed after hydrogenolysis (the samples used for this study were taken from the reaction employing diphenyl ether as the substrate). Remarkably, the morphology of $Ru_{15}Ni_{85}$ and $Rh_{15}Ni_{85}$ materials is largely preserved (Fig. S7 and S8†). ICP analysis was performed on the Ni_{100} NCs after washing with water revealing a Ni content of approx. 51 wt% (see ESI†), indicating that the CTAB remains attached to the Ni NCs (since CTAB is soluble in water). As a control experiment, the catalytic activity of the bimetallic NCs $M_{100-x}Ni_x$ (M = Ru or Rh and x = 85 or 50) was compared to monometallic NCs mixed in the same ratio in the transformation of diphenyl ether. The mixed NC systems are significantly less effective catalysts (typically 25–75% lower conversion) compared to the bimetallic NCs (Table S8†).

The standard Gibbs free energies of formation of all substrates and products and the standard Gibbs free energies of the reactions were estimated using a group contribution method. The method is specific to aqueous solution thermodynamics and describes meso- and macroscopic phenomena in the catalytic system that operates in water. The standard Gibbs free energies of all reactants and products were used to calculate standard Gibbs free energies of all the reactions, mapping the main possible pathways with formed intermediates and the corresponding thermodynamic parameters for the catalytic transformation of the model lignin dimers as shown in Fig. 5 (also see Fig. S9 and Table S9†). From the thermodynamic calculations all hydrogenation reactions appear to be less thermodynamically favourable than the hydrogenolysis. Specifically, for the hydrogenolysis of the cyclohexyl-phenyl ether the standard Gibbs energy of reaction showed that the formation of benzene and cyclohexanol are favoured over the formation of cyclohexane and phenol, which is in agreement with the obtained catalytic results.

Several substituted ether compounds (with C2-β-*O*-4 linkages) were also studied and the major products isolated (Fig. 6 and Table S10†). The $Ru_{15}Ni_{85}$ and $Rh_{15}Ni_{85}$ nanocatalysts completely convert the biaryl ethers containing hydroxy, keto or methoxy groups into monomers. With the $Ru_{15}Ni_{85}$ NCs hydrogenation of the arene ring is also observed resulting in cyclohexanol as a main product in 91% and 71% yield for 2-phenoxy-1-phenylethanol and 2-phenoxy-1-phenylethanone, respectively. In contrast, $Rh_{15}Ni_{85}$ NCs afford 1-(hydroxyethyl) benzene and phenol as the major products, *i.e.* 78 and 67% yield

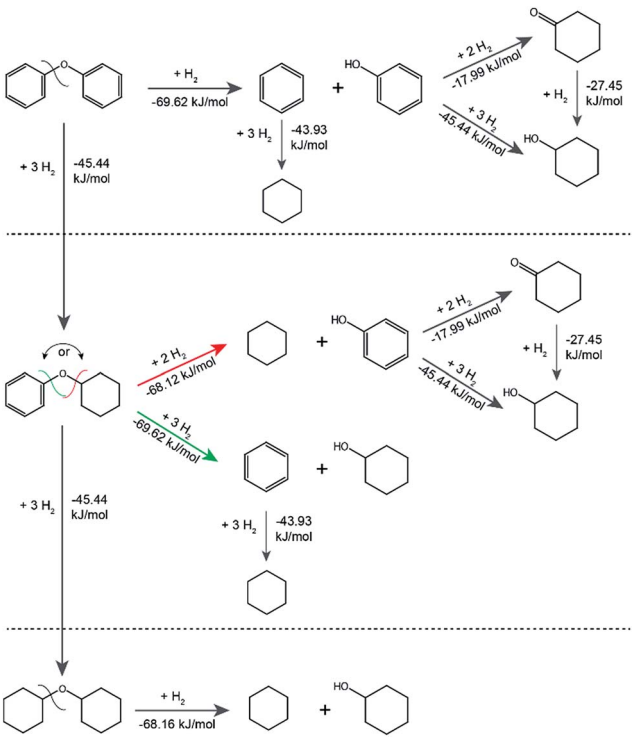

Fig. 5 Possible pathways and standard Gibbs free energies of reaction for the hydrogenolysis/hydrogenation of the model dimers (diphenyl ether, cyclohexyl phenyl ether and dicyclohexyl ether) in aqueous solution.

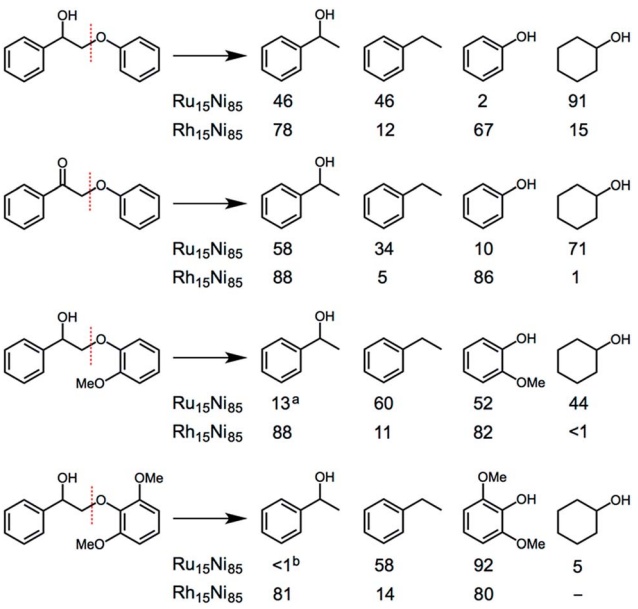

Fig. 6 Comparison of the main products obtained from the catalytic transformation of substituted ether compounds using $Ru_{15}Ni_{85}$ and $Rh_{15}Ni_{85}$ nanocatalysts. Conditions: aromatic ether (0.189 mmol), catalyst (5 mol%, 0.00945 mmol), H_2O (1 mL), H_2 (1 atm), 16 h, 95 °C. [a,b]In addition the hydrogenated derivative, 1-cyclohexylethanol, was also observed (12%[a] and 22%[b]). Full details are provided in Table S10.†

for 2-phenoxy-1-phenylethanol or 88 and 86% yield for 2-phenoxy-1-phenylethanone, respectively. The presence of *ortho*-methoxy groups significantly reduces the extent of hydrogenation, which has been noted previously, *i.e.* with arene hydrogenation catalysts that compare benzene, toluene and methoxybenzene substrates.[17] The ability of the $M_{15}Ni_{85}$ (M = Ru or Rh) NCs to transform beech wood was also validated, albeit under more forcing conditions, leading to a conversion of 57% with the formation of four main aromatic monomers in yields of up to 24% (Table S11†).

From the catalytic data, it would appear that the Ni is largely responsible for the hydrogenolysis reaction whereas the Ru and Rh are predominantly involved in the hydrogenation of the aromatic rings, as the extent of hydrogenation is higher at higher loadings of the precious metals. Several recent reports describe the hydrogenolysis of various C–O bonds using mostly *in situ* generated homogenous Ni catalysts.[13a,18] Some of these catalysts were used to activate aryl C(sp^2)–O bonds in different substrates,[18b,18c] and others were able to activate both aryl C(sp^2)–O and benzylic C(sp^3)–O bonds.[13a,18d–i] It is interesting to establish the activity and selectivity of the catalysts when both bond types are present. Hartwig *et al.* tested their catalyst on two compounds in the same reaction, one with an aryl C(sp^2)–O and the other with a benzylic C(sp^3)–O bond, and observed higher performance for the activation of aryl C(sp^2)–O bond.[13a] Similarly, Martin *et al.* observed the hydrogenolysis of stronger aryl C(sp^2)–O bonds in preference to benzylic C(sp^3)–O bonds, both present in the same substrate.[18d] Apparently, the selection of Ni precursors and ligands play an important role for the activation of each bond type. Accordingly, Shi *et al.* were able to selectively activate one of the bonds present in the same molecule, aryl C(sp^2)–O or benzylic C(sp^3)–O, by changing the ligands of the Ni catalyst.[18i] The substrates used in our work contain both type of bonds (the 4-*O*-5 linkage contains only aryl C(sp^2)–O bonds, whereas in α-*O*-4 and β-*O*-4 linkages both C(sp^2)–O and C(sp^3)–O bonds are present). In the presence of both bond types in the α-*O*-4 and β-*O*-4 linkages, the $Ru_{100-x}Ni_x$ and $Rh_{100-x}Ni_x$ NCs preferentially catalyse the hydrogenolysis of C(sp^3)–O bonds relative to C(sp^2)–O bonds (see Tables S2–S5†).

Moreover, following scission of the C–O linkages in the aryl ether substrates, hydrogenation of the aromatic ring in phenol takes place more efficiently than that of ethylbenzene and toluene. This is probably not only due to the intrinsic higher reactivity of the aromatic ring in phenol, but also due to stronger substrate–catalyst interactions, *i.e.* coordination of the oxygen heteroatom to the metal surface,[19] and enhanced mass transfer of phenol since it has a higher polarity and hence solubility in water. Combined, these effects increase the contact time of phenol with the catalyst surface and decreased activation barrier leading to increased levels of hydrogenation.

In summary, we have shown that Ru–Ni and Rh–Ni nanocatalysts coated with CTAB, a phase transfer agent, efficiently catalyze the hydrogenolysis of a variety of C–O bonds in a range of different substrates. These catalysts operate in water in the absence of additional reagents, which is advantageous in terms of sustainability,[20] but also ideal for the transformation of substrates present in or derived from biomass.

Conflicts of interest

There are no conflicts to declare.

Acknowledgements

We thank Swiss National Science Foundation National Research Programme (NRP 66) for financial support.

Notes and references

1 (*a*) C. Li, X. Zhao, A. Wang, G. W. Huber and T. Zhang, *Chem. Rev.*, 2015, **115**, 11559–11624; (*b*) P. J. Deuss and K. Barta, *Coord. Chem. Rev.*, 2016, **306**(Part 2), 510–532.

2 N. Yan and P. J. Dyson, *Curr. Opin. Chem. Eng.*, 2013, **2**, 178–183.

3 (*a*) P. Bi, J. Wang, Y. Zhang, P. Jiang, X. Wu, J. Liu, H. Xue, T. Wang and Q. Li, *Bioresour. Technol.*, 2015, **183**, 10–17; (*b*) H. Wang, H. Ruan, H. Pei, H. Wang, X. Chen, M. P. Tucker, J. R. Cort and B. Yang, *Green Chem.*, 2015, **17**, 5131–5135; (*c*) H. Wang, L. Zhang, T. Deng, H. Ruan, X. Hou, J. R. Cort and B. Yang, *Green Chem.*, 2016, **18**, 2802–2810.

4 (*a*) J. E. Holladay, J. F. White, J. J. Bozell and D. Johnson, *Top Value-Added Chemicals from Biomass – Volume II—Results of Screening for Potential Candidates from Biorefinery Lignin*, Report PNNL-16983, United States, 2007; (*b*) F. G. Calvo-Flores and J. A. Dobado, *ChemSusChem*, 2010, **3**, 1227–1235; (*c*) D. Stewart, *Ind. Crops Prod.*, 2008, **27**, 202–207; (*d*) D. R. Vardon, M. A. Franden, C. W. Johnson, E. M. Karp, M. T. Guarnieri, J. G. Linger, M. J. Salm, T. J. Strathmann and G. T. Beckham, *Energy Environ. Sci.*, 2015, **8**, 617–628.

5 Q. Song, F. Wang, J. Cai, Y. Wang, J. Zhang, W. Yu and J. Xu, *Energy Environ. Sci.*, 2013, **6**, 994–1007.

6 (*a*) T. Parsell, S. Yohe, J. Degenstein, T. Jarrell, I. Klein, E. Gencer, B. Hewetson, M. Hurt, J. I. Kim, H. Choudhari, B. Saha, R. Meilan, N. Mosier, F. Ribeiro, W. N. Delgass, C. Chapple, H. I. Kenttamaa, R. Agrawal and M. M. Abu-Omar, *Green Chem.*, 2015, **17**, 1492–1499; (*b*) C. S. Lancefield and N. J. Westwood, *Green Chem.*, 2015, **17**, 4980–4990; (*c*) N. Yan, C. Zhao, P. J. Dyson, C. Wang, L.-t. Liu and Y. Kou, *ChemSusChem*, 2008, **1**, 626–629; (*d*) T. vom Stein, T. den Hartog, J. Buendia, S. Stoychev, J. Mottweiler, C. Bolm, J. Klankermayer and W. Leitner, *Angew. Chem., Int. Ed.*, 2015, **54**, 5859–5863; (*e*) M. C. Haibach, N. Lease and A. S. Goldman, *Angew. Chem., Int. Ed.*, 2014, **53**, 10160–10163.

7 S. Constant, H. L. J. Wienk, A. E. Frissen, P. d. Peinder, R. Boelens, D. S. van Es, R. J. H. Grisel, B. M. Weckhuysen, W. J. J. Huijgen, R. J. A. Gosselink and P. C. A. Bruijnincx, *Green Chem.*, 2016, **18**, 2651–2665.

8 F. S. Chakar and A. J. Ragauskas, *Ind. Crops Prod.*, 2004, **20**, 131–141.

9 (*a*) Y. R. Luo, *Comprehensive Handbook of Chemical Bond Energies*, CRC Press, Boca Raton, FL, 2007; (*b*) M. W. Jarvis, J. W. Daily, H.-H. Carstensen, A. M. Dean, S. Sharma, D. C. Dayton, D. J. Robichaud and M. R. Nimlos, *J. Phys.*

Chem. A, 2011, **115**, 428–438; (*c*) A. Beste and A. C. Buchanan, *J. Org. Chem.*, 2009, **74**, 2837–2841; (*d*) S. Kim, S. C. Chmely, M. R. Nimlos, Y. J. Bomble, T. D. Foust, R. S. Paton and G. T. Beckham, *J. Phys. Chem. Lett.*, 2011, **2**, 2846–2852.

10 (*a*) B. Güvenatam, O. Kurşun, E. H. J. Heeres, E. A. Pidko and E. J. M. Hensen, *Catal. Today*, 2014, **233**, 83–91; (*b*) C. R. Lee, J. S. Yoon, Y.-W. Suh, J.-W. Choi, J.-M. Ha, D. J. Suh and Y.-K. Park, *Catal. Commun.*, 2012, **17**, 54–58; (*c*) V. Molinari, G. Clavel, M. Graglia, M. Antonietti and D. Esposito, *ACS Catal.*, 2016, **6**, 1663–1670; (*d*) J. Zhang, J. Teo, X. Chen, H. Asakura, T. Tanaka, K. Teramura and N. Yan, *ACS Catal.*, 2014, **4**, 1574–1583; (*e*) J. Zhang, M. Ibrahim, V. Collière, H. Asakura, T. Tanaka, K. Teramura, K. Philippot and N. Yan, *J. Mol. Catal. A: Chem.*, 2016, **422**, 188–197; (*f*) J. K. Kim, J. K. Lee, K. H. Kang, J. W. Lee and I. K. Song, *J. Mol. Catal. A: Chem.*, 2015, **410**, 184–192; (*g*) Y.-C. Lin, C.-L. Li, H.-P. Wan, H.-T. Lee and C.-F. Liu, *Energy Fuels*, 2011, **25**, 890–896; (*h*) T. H. Parsell, B. C. Owen, I. Klein, T. M. Jarrell, C. L. Marcum, L. J. Haupert, L. M. Amundson, H. I. Kenttamaa, F. Ribeiro, J. T. Miller and M. M. Abu-Omar, *Chem. Sci.*, 2013, **4**, 806–813; (*i*) Q. Xia, Z. Chen, Y. Shao, X. Gong, H. Wang, X. Liu, S. F. Parker, X. Han, S. Yang and Y. Wang, *Nat. Commun.*, 2016, **7**, 11162; (*j*) P. J. Deuss, M. Scott, F. Tran, N. J. Westwood, J. G. de Vries and K. Barta, *J. Am. Chem. Soc.*, 2015, **137**, 7456–7467; (*k*) Z. Li, R. S. Assary, A. C. Atesin, L. A. Curtiss and T. J. Marks, *J. Am. Chem. Soc.*, 2014, **136**, 104–107; (*l*) J. Lu, M. Wang, X. Zhang, A. Heyden and F. Wang, *ACS Catal.*, 2016, **6**, 5589–5598.

11 (*a*) A. K. Deepa and P. L. Dhepe, *ACS Catal.*, 2015, **5**, 365–379; (*b*) X. Huang, C. Atay, T. I. Korányi, M. D. Boot and E. J. M. Hensen, *ACS Catal.*, 2015, **5**, 7359–7370; (*c*) J. He, C. Zhao and J. A. Lercher, *J. Am. Chem. Soc.*, 2012, **134**, 20768–20775; (*d*) S. Kasakov, H. Shi, D. M. Camaioni, C. Zhao, E. Barath, A. Jentys and J. A. Lercher, *Green Chem.*, 2015, **17**, 5079–5090; (*e*) S. K. Singh and J. D. Ekhe, *RSC Adv.*, 2014, **4**, 27971–27978; (*f*) W. Song, Y. Liu, E. Barath, C. Zhao and J. A. Lercher, *Green Chem.*, 2015, **17**, 1204–1218; (*g*) M. D. Karkas, B. S. Matsuura, T. M. Monos, G. Magallanes and C. R. J. Stephenson, *Org. Biomol. Chem.*, 2016, **14**, 1853–1914; (*h*) Y.-Y. Wang, L.-L. Ling and H. Jiang, *Green Chem.*, 2016, **18**, 4032–4041; (*i*) X. Wang and R. Rinaldi, *Catal. Today*, 2016, **269**, 48–55; (*j*) C. S. Lancefield, O. S. Ojo, F. Tran and N. J. Westwood, *Angew. Chem., Int. Ed.*, 2015, **54**, 258–262; (*k*) P. Ferrini and R. Rinaldi, *Angew. Chem., Int. Ed.*, 2014, **53**, 8634–8639; (*l*) R. Ma, W. Hao, X. Ma, Y. Tian and Y. Li, *Angew. Chem., Int. Ed.*, 2014, **53**, 7310–7315; (*m*) T. Prasomsri, M. Shetty, K. Murugappan and Y. Roman-Leshkov, *Energy Environ. Sci.*, 2014, **7**, 2660–2669; (*n*) X. Cui, H. Yuan, K. Junge, C. Topf, M. Beller and F. Shi, *Green Chem.*, 2017, **19**, 305–310.

12 L. Chen, J. Xin, L. Ni, H. Dong, D. Yan, X. Lu and S. Zhang, *Green Chem.*, 2016, **18**, 2341–2352.

13 (*a*) A. G. Sergeev and J. F. Hartwig, *Science*, 2011, **332**, 439–443; (*b*) A. G. Sergeev, J. D. Webb and J. F. Hartwig, *J. Am. Chem. Soc.*, 2012, **134**, 20226–20229; (*c*) F. Gao, J. D. Webb and J. F. Hartwig, *Angew. Chem., Int. Ed.*, 2016, **55**, 1474–1478.

14 N. I. Saper and J. F. Hartwig, *J. Am. Chem. Soc.*, 2017, **139**, 17667–17676.

15 (*a*) S. Hou, C. Xie, F. Yu, B. Yuan and S. Yu, *RSC Adv.*, 2016, **6**, 54806–54811; (*b*) X. Cui, A.-E. Surkus, K. Junge, C. Topf, J. Radnik, C. Kreyenschulte and M. Beller, *Nat. Commun.*, 2016, **7**, 11326.

16 H. Konnerth, J. Zhang, D. Ma, M. H. G. Prechtl and N. Yan, *Chem. Eng. Sci.*, 2015, **123**, 155–163.

17 P. J. Dyson, *Dalton Trans.*, 2003, 2964–2974, DOI: 10.1039/B303250G.

18 (*a*) J. Cornella, C. Zarate and R. Martin, *Chem. Soc. Rev.*, 2014, **43**, 8081–8097; (*b*) J. Cornella, E. Gómez-Bengoa and R. Martin, *J. Am. Chem. Soc.*, 2013, **135**, 1997–2009; (*c*) J. Cornella, P. Jackson Evan and R. Martin, *Angew. Chem., Int. Ed.*, 2015, **54**, 4075–4078; (*d*) P. Álvarez-Bercedo and R. Martin, *J. Am. Chem. Soc.*, 2010, **132**, 17352–17353; (*e*) A. Correa, T. León and R. Martin, *J. Am. Chem. Soc.*, 2014, **136**, 1062–1069; (*f*) A. Correa and R. Martin, *J. Am. Chem. Soc.*, 2014, **136**, 7253–7256; (*g*) C. Zarate, R. Manzano and R. Martin, *J. Am. Chem. Soc.*, 2015, **137**, 6754–6757; (*h*) C. Zarate, M. Nakajima and R. Martin, *J. Am. Chem. Soc.*, 2017, **139**, 1191–1197; (*i*) B.-T. Guan, S.-K. Xiang, B.-Q. Wang, Z.-P. Sun, Y. Wang, K.-Q. Zhao and Z.-J. Shi, *J. Am. Chem. Soc.*, 2008, **130**, 3268–3269.

19 D. Garcia-Pintos, J. Voss, A. D. Jensen and F. Studt, *J. Phys. Chem. C*, 2016, **120**, 18529–18537.

20 (*a*) P. G. Jessop, F. Joó and C.-C. Tai, *Coord. Chem. Rev.*, 2004, **248**, 2425–2442; (*b*) S. Bulut, Z. Fei, S. Siankevich, J. Zhang, N. Yan and P. J. Dyson, *Catal. Today*, 2015, **247**, 96–103.